J Biol Inorg Chem (2010) 15:409–420
DOI 10.1007/s00775-009-0613-6

ORIGINAL PAPER

# An NMR structural study of nickel-substituted rubredoxin

**Brian J. Goodfellow · Iven C. N. Duarte · Anjos L. Macedo · Brian F. Volkman · Sofia G. Nunes · I. Moura · John L. Markley · José J. G. Moura**

Received: 22 March 2009 / Accepted: 10 November 2009 / Published online: 8 December 2009


**Abstract** The Ni(II) and Zn(II) derivatives of *Desulfovibrio vulgaris* rubredoxin (DvRd) have been studied by NMR spectroscopy to probe the structure at the metal centre. The $\beta CH_2$ proton pairs from the cysteines that bind the Ni(II) atom have been identified using 1D nuclear Overhauser enhancement (NOE) difference spectra and sequence specifically assigned via NOE correlations to neighbouring protons and by comparison with the published X-ray crystal structure of a Ni(II) derivative of *Clostridium pasteurianum* rubredoxin. The solution structures of DvRd(Zn) and DvRd(Ni) have been determined and the paramagnetic form refined using pseudocontact shifts. The determination of the magnetic susceptibility anisotropy tensor allowed the contact and pseudocontact contributions to the observed chemical shifts to be obtained. Analysis of the pseudocontact and contact chemical shifts of the cysteine H$\beta$ protons and backbone protons close to the metal centre allowed conclusions to be drawn as to the geometry and hydrogen-bonding pattern at the metal binding site. The importance of NH–S hydrogen bonds at the metal centre for the delocalization of electron spin density is confirmed for rubredoxins and can be extrapolated to metal centres in Cu proteins: amicyanin, plastocyanin, stellacyanin, azurin and pseudoazurin.

**Keywords** NMR · Rubredoxin · [Fe–4S] centre · Paramagnetic protein · Nickel

**Abbreviations**

| | |
|---|---|
| CpRd | *Clostridium pasteurianum* rubredoxin |
| DvRd | *Desulfovibrio vulgaris* rubredoxin |
| HSQC | Heteronuclear single quantum coherence |
| MST | Magnetic susceptibility anisotropy tensor |
| NOE | Nuclear Overhauser enhancement |
| NOESY | Nuclear Overhauser enhancement spectroscopy |
| PCS | Pseudocontact shift |
| PDB | Protein Data Bank |
| PfRd | *Pyrococcus furiosus* rubredoxin |
| Rd | Rubredoxin |
| RMSD | Root-mean-square deviation |
| TOCSY | Total correlation spectroscopy |

**Electronic supplementary material** The online version of this article (doi:10.1007/s00775-009-0613-6) contains supplementary material, which is available to authorized users.

B. J. Goodfellow (✉) · I. C. N. Duarte
CICECO, Departamento de Química,
Universidade Aveiro,
3810-193 Aveiro, Portugal
e-mail: brian.goodfellow@ua.pt

A. L. Macedo · I. Moura · J. J. G. Moura
REQUIMTE/CQFB, Departamento de Química,
Faculdade de Ciências e Tecnologia,
Universidade Nova de Lisboa,
2829-516 Caparica, Portugal
e-mail: jose.moura@dq.fct.unl.pt

B. F. Volkman
Department of Biochemistry,
Medical College of Wisconsin,
Milwaukee, WI 53226, USA

S. G. Nunes
Valencia Infertility Institute (IVI),
Valencia, Spain

J. L. Markley
Department of Biochemistry,
171A Biochemistry Addition,
University of Wisconsin,
433 Babcock Drive,
Madison, WI 53706-1544, USA

## Introduction

Rubredoxin belongs to the class of Fe–S proteins containing one Fe atom tetrahedrally coordinated to four cysteinyl S atoms. Rubredoxin, isolated from sulphate-reducing bacteria, has a molecular mass of approximately 6–7 kDa and the metal atom in the native state is high-spin $Fe^{3+}$ ($S = 5/2$). The reduced state has high-spin $Fe^{2+}$ ($S = 2$). The cysteines that bind the metal have a conserved sequence of the type $-CX_1X_2CG-//-CX_3X_4CG$. More than 20 rubredoxin structures are to be found in the Protein Data Bank (PDB), including two very high resolution structures at (0.7 Å) from a *Pyrococcus abyssi* mutant and from *Desulfovibrio gigas* [1, 2].

When NMR is applied to paramagnetic metalloproteins, a number of problems can be encountered, including large hyperfine shifts and extensive line broadening which can result in loss of NMR signals close to the metal centre. This problem is illustrated for the solution structure of the oxidized and reduced Fe forms of *Clostridium pasteurianum* rubredoxin (CpRd), where constraints near the metal centre are almost absent, resulting in disorder close to the metal [3]. However, compared with tetrahedral Fe(II) or Fe(III), where signal loss is extensive, tetrahedral Ni(II), owing to its favourable electronic relaxation properties, allows even the H$\beta$ resonances of the coordinating cysteines to be observed, albeit at low field [4]. Nowadays, the presence of a paramagnetic centre can be used to obtain pseudocontact shifts (PCSs) and residual dipolar couplings that can be combined with traditional nuclear Overhauser enhancement spectroscopy (NOESY) data for structure determination [5, 6]. Even if the system under study does not have an inherent metal centre, one can be added to take advantage of these data [7, 8]. As rubredoxin is a small accessible protein with easy metal replacement, a number of studies have used rubredoxin as a model to attempt new structure determination approaches using PCSs and residual dipolar couplings [9–15]. Also, for CpRd(Fe) the relaxation properties and chemical shifts of hyperfine-shifted resonances have given information on the state of hydrogen bonding at and around the metal centre and studies involving theoretical calculations have shown a dependence of the redox potential on hydrogen-bond strength (essentially distance) [16–21]. The magnetic susceptibility anisotropy tensor (MST) for oxidized and reduced CpRd(Fe) has been determined and it was shown that redox-dependant chemical shift changes for protons farther than approximately 11 Å from the Fe atom were due to changes in the MST and not from structural modifications when going from the oxidized to the reduced state [22]. Also, very recently, an almost complete assignment of the $^{15}N$ and $^{13}C$ signals from oxidized and reduced CpRd(Fe) was carried out using selective isotope labelling and novel techniques for detecting fast relaxing resonances [23].

The importance of the hydrogen-bonding network in rubredoxins has also been illustrated in a study of the Zn(II) forms of CpRd and *P. furiosus* rubredoxin (PfRd), where it was suggested that the thermostability of PfRd results from a subtle redistribution of hydrogen bonds in the $\beta$-sheet sections of the protein and at the metal centre [11]. A study of diamagnetic derivatives of CpRd and PfRd [24] has further indicated that the symmetry of the hydrogen bonds to the metal-coordinated S atoms is more closely maintained in the hyperthermophile *P. furiosus*.

Ni(II)-containing enzymes such as urease and hydrogenase are involved in important biochemical processes and as such they have been extensively studied. NiFe hydrogenase and carbon monoxide dehydrogenase both have a tetrahedral Ni(II) centre bound to four S atoms at the active site, a centre relatively rare in biochemistry [25]. In the past, to study the mechanistic reaction of these (or of any metal-containing) proteins, theoretical models were used. As metal substitution is easily carried out for rubredoxin, the Ni(II) derivative is a candidate for a model of the active site of these enzymes. There are very few NMR solution structures of Ni(II)-containing proteins (PDB entries 1ZRR [26], 2DEF [27] and 2GQK [28]) and the only Ni(II)-containing rubredoxin structure determined up until now is the X-ray structure of CpRd(Ni). This was resolved at relatively low resolution (2 Å) and therefore no detailed analysis was carried out; however, the data indicate that the overall structures of the native Fe and Ni(II) forms are very similar [29].

Other metalloproteins containing Ni(II) studied by NMR include the Ni(II)-substituted forms of azurin [30–33], amicyanin [34], pseudoazurin [35], stellacyanin [36] and umecyanin [37]. With use of the crystal structures of the Cu and Ni(II) forms of azurin it was possible to calculate the axial and rhombic components of the MST. It was found, for instance, that the Ni(II) form had a lower anisotropy than Co(II) form.

To probe the structure in solution of Ni(II)-substituted *D. vulgaris* rubredoxin (DvRd), PCSs were obtained and combined with NOESY data. By obtaining the MST for DvRd(Ni), we could predict the PCS contribution to the chemical shifts of nuclei close to the metal centre and subsequently extract their contact shift contribution. This not only allowed additional assignments to be made, but it also allowed the delocalization of unpaired electron spin density onto nuclei near the metal centre to be estimated. Conclusions could subsequently be drawn as to the geometry of the hydrogen-bonding network at the metal centre in this Ni derivative.

## Materials and methods

### Protein purification and metal derivative preparation

Unlabelled DvRd was isolated and purified according to the method of Bruschi et al. [38]. Isotopic labelling of rubredoxin was carried out using a process identical to that described in Goodfellow et al. [39]. The Ni form of rubredoxin was prepared according to the method of Moura et al. [4]. The NMR samples were prepared by exchange into phosphate buffer (10 mM, pH 7.2) containing 5% $D_2O$ and by repeated concentration/dilution using a Centricon YM3 concentrator (Amicon). The final sample concentrations were 1–2 mM.

### NMR spectroscopy

For structure determination, backbone $^{1}H$ and $^{15}N$ resonances [for the Zn(II) and Ni(II) forms of DvRd] were assigned using manual methods with data from the following experiments: [$^{1}H$–$^{15}N$] heteronuclear single quantum coherence (HSQC), 2D NOESY (mixing time, 150 ms), 2D total correlation spectroscopy (TOCSY) (mixing time, 70 ms), $^{15}N$-edited NOESY–HSQC (mixing time, 150 ms) and $^{15}N$-edited TOCSY–HSQC (mixing time, 70 ms). A fast-recycle 2D NOESY spectrum with 20-ms mixing time, 300-ms recycle delay and 80-ppm sweep width was also used for assignment in the case of DvRd(Ni). These spectra were obtained with either a Bruker DRX500 or a Bruker DRX600 (at the National Magnetic Resonance Facility at Madison) spectrometer using TBI and TXI probes, respectively. All spectra were processed and analysed using NMRPipe [40], Sparky [41] or XEASY [42] software programs. Chemical shifts were referenced, either directly or indirectly, to 2,2-dimethylsilapentane-5-sulphonic acid at 0 ppm [43].

One-dimensional nuclear Overhauser enhancement (NOE) difference spectra were recorded at 400 and 500 MHz (at the Portuguese National NMR Facility at Caparica and Aveiro, respectively) using the super-WEFT pulse sequence [44] for water suppression (180-*t*-90-AQ) with *t* values and recycle times of approximately 150 ms. Selective saturation of the resonances was made during the delay time *t*. Difference spectra were obtained by subtracting the off-resonance spectra from the on-resonance spectra [45, 46].

### Structure determination

Distance constraints for the DvRd(Zn) structure were obtained from 2D NOESY and 3D $^{15}N$-edited NOESY–HSQC spectra. Structures were generated using the torsion angle dynamics program CYANA [47], followed by manual refinement of the NOE assignments to eliminate consistent violations. The coordinates and experimental constraints have been deposited in the PDB, entry 2QL0, and the chemical shift assignments have been deposited in the Biological Magnetic Resonance Data Bank (15374). The structure of paramagnetic DvRd(Ni) was determined using distance constraints from 1D NOE, 2D NOESY and 3D $^{15}N$-edited NOESY–HSQC spectra. PCS restraints were included using the program PSEUDYANA [48], which is based on DYANA 1.5 [49]. The coordinates and experimental constraints for this form have been deposited in the PDB, entry 2KKD, and the chemical shift assignments have been deposited in the Biological Magnetic Resonance Data Bank (15375). The minimization parameters used for the DYANA and PSEUDYANA runs are described in "Results".

The programs FANTASIAN [50] and NUMBAT [51] were used to calculate the MST parameters from PCS data. For the initial PCS tensor calculations, only shifts from residues farther than eight covalent bonds from the metal atom were used to avoid any possible contact shift contributions (including via hydrogen bonds, vide infra). The X-ray structures of the native Fe form of DvRd (8RXN) or the Ni(II) form of CpRd (1R0J) were used in the calculations. PCS isosurfaces were calculated using the program NUMBAT. PyMOL [52] was used for all manipulations of structures, for the addition of hydrogen atoms when required and for graphical representations.

## Results

### DvRd(Zn) solution structure

A total of 90% of the $^{1}H$ resonance assignments of DvRd(Zn) were obtained through standard procedures. From a total of 47 resonances in a [$^{1}H$–$^{15}N$]-HSQC spectrum, 44 result from main-chain NH groups and three from the side chains of N22 ($NH_2$) and W37 (NH$\varepsilon$). No resonances were observed for residues M1 and K2 owing to fast exchange of the amide group with the solvent under these experimental conditions.

The torsion angle dynamics program CYANA was used to calculate a family of low target function structures. The Zn(II) atom was included in the calculations by covalently linking it to the C6 S$\gamma$ atom and introducing three constraints for the other cysteine S$\gamma$ atoms. The tetrahedral geometry of the centre was achieved by constraining, with upper and lower constraints, the distance between the S atoms of the coordinating cysteines (all with a weighting of 1). This resulted in 12 distance constraints for the Zn(II) centre. These limits were calculated on the basis of the X-ray structure of oxidized DvRd(Fe). A final total of 581 distance constraints were used (intra 122, short 147, medium 121, long 203). A CYANA calculation from 200

starting structures gave a final family of 20, with an average target function value of 0.020 ± 0.003 Å$^2$. The global root-mean-square deviations (RMSD) for the family were 0.58 ± 0.18 and 1.00 ± 0.19 Å for backbone and heavy atoms, respectively. A comparison of the NMR structure closest to the mean structure and an X-ray structure of oxidized DvRd(Fe) gave a global backbone RMSD of 1.0 Å (excluding the N-terminus and two disordered loops: 18–25, 45–47). The RMSD per residue is given in the electronic supplementary material.

## Assignment of the Hβ cysteine protons in DvRd(Ni)

Figure 1 shows the low-field 400–100-ppm region of the $^1$H NMR spectra of DvRd(Ni), where eight nonexchangeable resonances can be seen (a–h). One-dimensional NOE difference spectra were recorded in $D_2O$ and indicated that the resonances a/c, b/d, e/h and f/g form four pairs of neighbouring protons (Table 1). As these peaks are not solvent-exchangeable and the cysteine Hβ protons can be expected to display the largest low-field shifts owing to their contact contribution, they can be assigned to the coordinating cysteines (C6, C9, C39 and C42 in rubredoxin). Similar observations have been made for reduced CpRd(Fe) for samples selectively labelled with [$^2$H$^\alpha$]Cys or [$^2$H$^\beta$]Cys [19]. A combination of four 1D NOE difference spectra and a 2D NOESY spectrum (20 ms) allowed sequence-specific assignment for the cysteine C6 (e/h) and C39 (f/g) Hβ protons. As only peaks g and h show NOEs to the Hζ and Hε protons of F49, stereospecific assignment of these peaks to the pro-S protons of C39 and C6, respectively, can be made (Table 1). By combining information from a 100-ms NOESY spectrum, we could also identify another 1D NOE (from the irradiation of peak h) as resulting from the $CH_3$ group of A44. This group is within 3.5 Å of Hβ of C39. The protons of the a/c and b/d pairs only show one NOE in the region 30–5 ppm. This is consistent with their assignment to either C9 or C42 as there are very few protons within 5 Å of these Hβ pairs. In both cases the closest proton to the Hβ pair is Hα of the same residue and therefore the most intense NOE observed in both spectra was identified as the Hα proton (data not shown). In this case it was impossible to sequentially or stereospecifically assign the Hβ protons since the intensities of both NOEs were similar.

## DvRd(Ni) solution structure

The initial resonance assignment of peaks from residues far from the metallic centre was straightforward using previously assigned residues from DvRd(Zn). As expected, for residues close to the metal centre, the assignment was more demanding. A combination of a 3D HSQC–NOESY spectrum and an HSQC–TOCSY spectrum allowed the assignment of the 2D [$^1$H–$^{15}$N]-HSQC spectrum of DvRd(Ni). Of 46 possible HN resonances, 33 were observed along with three resonances from the side chains of residues N22 ($NH_2$) and W37 (NHε). No NH resonances were observed for residues M1, K2, C6-Y11, C39 and V41-A44 in this spectrum (Fig. 2). To obtain the resonances of nuclei near the metallic centre, 2D NOESY and TOCSY experiments with a mixing time of 20 ms and a recycle time of 300 ms were performed. In this manner a significant number of additional hyperfine-shifted resonances were detected and assigned. One-dimensional NOE difference spectra acquired by irradiating the contact-shifted cysteine Hβ protons allowed further assignment. Final assignments were obtained after calculation of the MST and prediction of PCSs via the program FANTASIAN. After this process had been completed, there were only two residues (M1 and G10) for which there were no assigned resonances.

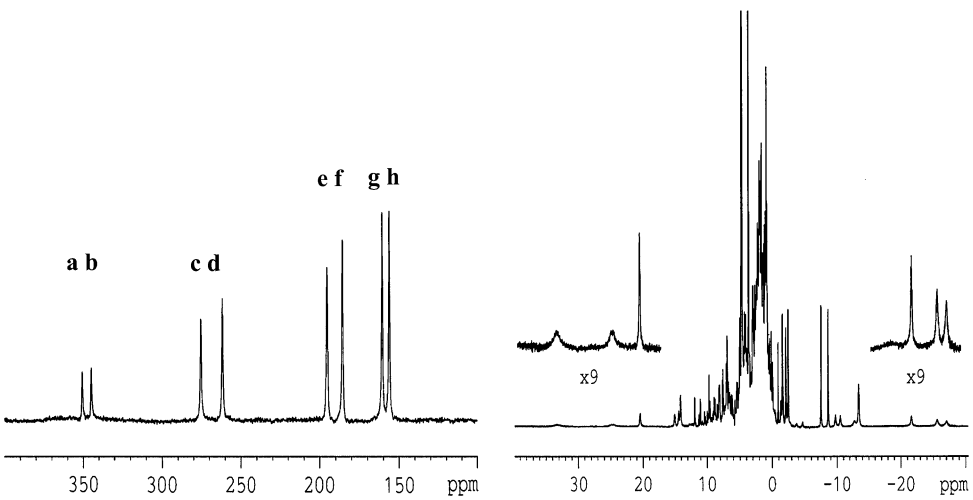


**Fig. 1** The 1D $^1$H NMR spectrum of the Ni(II) form of *Desulfovibrio vulgaris* rubredoxin (DvRd) at 302 K. The low-field contact-shifted Hβ protons from the four binding cysteines can be observed between 350 and 150 ppm (*a–h*). Other contact- and pseudocontact-shifted peaks can be seen outside the diamagnetic envelope up to +30 ppm and down to −30 ppm. The difference in peak intensity seen for the low-field shifted peaks is due to an uneven excitation profile

**Table 1** $^{1}$H NMR chemical shifts for the ligating cysteine H$\beta$ protons from the Ni(II) and Fe(II) forms of *Desulfovibrio vulgaris* rubredoxin (DvRd) and *Clostridium pasteurianum* rubredoxin (CpRd), respectively, and published chemical shifts for a number of Ni(II)-containing azurin-like proteins

| | H$\beta$ | $\delta_{obs}$ | $\delta_{1/2}$ | M–S$\gamma$–C$\beta$–C$\alpha$ | HN–SH bonds[a] |
|---|---|---|---|---|---|
| DvRd(Ni) | | | | | |
| C9/C42 | a(c) | 362 (279) | 321/320 | −94.35/−89.65$^{8RXN}$ | 1 |
| C42/C9 | b(d) | 360 (269) | 321/320 | −89.65/−94.35 | 1 |
| C6$^{proR}$ | e(h) | 198 (161) | 183 | −172.69 | 2 |
| C39$^{proR}$ | f(g) | 188 (167) | 178 | −175.33 | 2 |
| CpRd(Fe) | | | | | |
| C42$^{proS}$ | a(c) | 251 (233) | 242[b] | −83.8$^{5RXN}$ | 1 |
| C9$^{proS}$ | b(d) | 244 (233) | 239[b] | −90.5 | 1 |
| C6$^{proR}$ | e(h) | 196 (157) | 178[b] | −177.7 | 2 |
| C39$^{proR}$ | f(g) | 193 (159) | 176[b] | −178.2 | 2 |
| CpRd(Ni) | | | | | |
| C42 | | | | −84.7$^{1R0J}$ | 1[c] |
| C9 | | | | −95.2 | 1 |
| C6 | | | | −167.7 | 2 |
| C39 | | | | −178.8 | 2 |
| UMC | | | | | |
| C85$^{proS}$ | | 224 (167) | 196[d] | −169.6$^{1X9U}$ | 2 |
| AZ | | | | | |
| C112$^{proS}$ | | 238 (197) | 218[e] | −161.4$^{2AZA}$ | 2 |
| AZ | | | | | |
| C112$^{proS}$ | | 233 (187) | 210[f] | −171.0$^{4AZU}$ | 2 |
| AZ$^{M121Q}$ | | | | | |
| C112$^{proS}$ | | 237 (178) | 208[e] | 169.1$^{1URI}$ | 2 |
| AZ | | | | | |
| C112$^{proS}$ | | 238 (194) | 216[g] | −172.7$^{2CCW}$ | 2 |
| STC | | | | | |
| C87$^{proS}$ | | 197 (177) | 187[h] | −176.2$^{1JER-CsSTC}$ | 2 |
| PA | | | | | |
| C78$^{proS}$ | | 297 (274) | 285[i] | −169.2$^{1BQK}$ | 1 |
| AMI | | | | | |
| C93$^{proS}$ | | 254 (296) | 275[j] | −171.6$^{1ID2}$ | 1 |

Dihedral angles for C$\alpha$ of the cysteines ligating the metal atom in DvRd(Fe), CpRd(Ni) and CpRd(Fe) are taken from the X-ray structures 8RXN, 1R0J and 5RXN, respectively. The average NMR chemical shifts for the cysteine H$\beta$ protons in DvRd(Ni) and CpRd(Fe) are included along with the number of HN–S hydrogen bonds in which each cysteinyl S is involved. The structural data for the azurin-like proteins are for the native Cu forms and the NMR data are for the Ni(II) derivatives

*UMC* umecyanin, *AZ* azurin, *STC* stellacyanin, *PA* pseudoazurin, *AMI* amicyanin

[a] Within 2.8 Å

[b] $^{2}$H shifts from the reduced form, data taken from [19]

[c] 3.1 Å

[d] From [37]

[e] From [31]

[f] From [33]

[g] From [32]

[h] From [36]

[i] From [35]

[j] From [34]

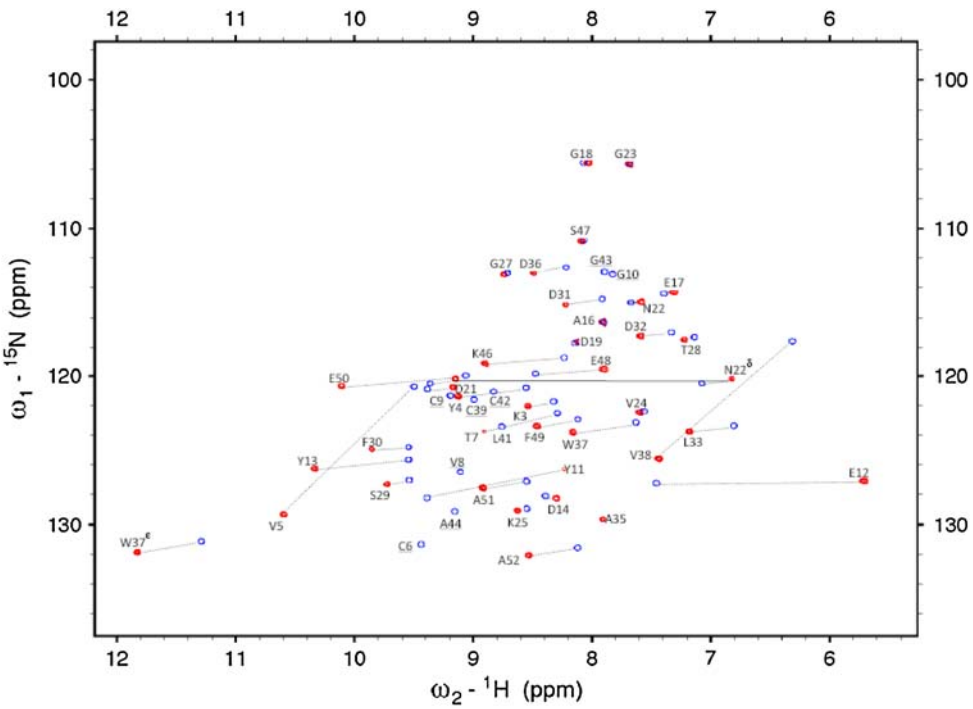


**Fig. 2** The [$^1$H–$^{15}$N] heteronuclear single quantum coherence spectra of DvRd(Zn) (*blue*) and DvRd(Ni) (*red*) at 296 K in phosphate buffer at pH 7.2. Assignments are indicated along with selected hyperfine shifts

**Table 2** The magnetic susceptibility anisotropy tensors calculated using experimental pseudocontact shifts from DvRd(Ni) and the coordinates from the DvRd(Ni) NMR structure and the DvRd(Fe) and CpRd(Ni) X-ray structures

| | $\Delta\chi_{ax}$ ($\times 10^{-32}$ m$^3$) | $\Delta\chi_{rh}$ ($\times 10^{-32}$ m$^3$) | $\alpha$ | $\beta$ | $\gamma$ |
|---|---|---|---|---|---|
| DvRd(Fe) (8RXN) | −3.61 (0.10) | −0.88 (0.05) | 148 (0.3) | 69 (0.6) | 16 (1.8) |
| CpRd(Ni) (1R0J) | −3.41 (0.08) | −0.92 (0.05) | 57 (0.5) | 96 (0.4) | 59 (1.8) |
| DvRd(Ni) (2KKD) | −3.86 (0.09) | −0.62 (0.07) | 174 (0.6) | 121 (0.9) | 81 (2.9) |

The errors presented are standard deviations calculated from 100 sets of randomized (0.1 Å standard deviation) atom coordinates via NUMBAT

A family of structures was calculated using the program PSEUDYANA [48], which allows for the inclusion of PCSs in a torsion angle dynamics protocol. The PCSs of the $^1$H and $^{15}$N nuclei were determined by subtracting the diamagnetic contribution from the total hyperfine shifts, using the diamagnetic DvRd(Zn) analogue. Possible contact shift contributions (via covalent and hydrogen bonds) were avoided by excluding PCSs from any nucleus within eight covalent bonds of the metal, i.e. residues V5-Y11 and V38-A44. A total of 147 $^1$H and $^{15}$N PCSs were initially used as restraints. The initial MST for the structure calculations was determined using the program FANTASIAN. Atomic coordinates from the X-ray structure of the Fe form of DvRd (8RXN) and the experimental PCSs served as input for this step. The subsequent calculations in PSEUDYANA used experimental PCSs and calculated NMR structures in the minimization protocol.

The Ni(II) atom was included in the calculations using a series of linker residues placed at the C-terminus with additional constraints between the metal and the cysteine S$\gamma$ and C$\beta$ atoms and between all cysteine S$\gamma$ atoms. To keep the centre in a tetrahedral environment, these constraints were given a weighting of 20. In addition, experimental constraints from the 2D and 3D NOESY spectra and from the fast-recycle 2D NOESY and the 1D NOE difference experiments were included to give a total of 529 constraints (161 intra, 95 short, 96 medium, 177 long). The experimental PCSs were included with a weighting of 5 compared with the NOE constraints. This was due to lower weightings giving poorer definition at the metal atom. From an initial total of 800 conformers, 15 gave a lowest target function of 3.65 Å$^2$. This value is rather high; target function values of less than 1.5 Å$^2$ are normally considered as acceptable. However, inspecting the constraint violations indicated that the PCSs for a number of side-chain resonances and many $^{15}$N resonances were being violated. It has been noted previously that the use of $^{15}$N PCSs can be problematic. A study of the use of lanthanide-based PCSs for structure assignment [53] found that for two diamagnetic reference compounds although backbone $^1$H chemical shifts did not change between apo-$\varepsilon$186 and $\varepsilon$186(La$^{3+}$), the $^{15}$N shifts varied considerably. Also, owing

to the small size of rubredoxin, a large percentage of the residues are surface-exposed, with the possibility of motional averaging. Therefore, the calculation was repeated using only backbone PCSs and no $^{15}$N PCSs, giving a total of 66 restraints. PSEUDYANA does not minimize the magnitude of the MST during the structure calculation, only its position and orientation. Therefore, after an initial family of structures had been calculated, a new MST was calculated and this tensor was used in a new round of structure calculations [54]. This process was repeated five times, resulting in an average MST with a magnitude of $\chi_{ax} = (-3.85 \pm 0.02) \times 10^{-32}$ and $\chi_{rh} = (-0.62 \pm 0.02) \times 10^{-32}$ m$^3$. The family of structures with the MST closest to this value was subsequently used.

This family of 15 structures with a maximum target function of 1.34 Å$^2$ was obtained from an initial total of 400 conformations. Here there were three NOE constraints greater than 0.43 Å. The global RMSD for the family was 0.96 ± 0.22 Å for the backbone atoms and 1.52 ± 0.22 Å for the heavy atoms. The constraints and RMSD per residue are given in the electronic supplementary material.

### Determination of the MST in DvRd(Ni)

The program NUMBAT was used to calculate the MST parameters for three different rubredoxin structures: DvRd(Fe) (8RXN); CpRd(Ni) (1R0J); and DvRd(Ni) (2KKD). Experimental PCS data from DvRd(Ni) were used in conjunction with the corresponding atomic coordinates. For these tensor calculations only the reduced set of backbone PCSs, excluding residues further than eight covalent bonds from the metal atom, were used to avoid any possible contact shift contribution. The $^{15}$N resonances were also excluded. The origin of the MST was constrained to the coordinates of the metal atom in the structures used for the calculations. The resulting tensors and their orientations are shown in Table 2. By plotting experimental PCSs and PCSs calculated from the fitted MST for all the PCSs used in the calculation and the PCSs from nuclei within eight covalent bonds of the Ni(II) atom (Fig. 3), the presence of contact shift contributions to the observed chemical shifts in DvRd(Ni) can be seen (vide infra). A chemical shift PCS isosurface at ±1 ppm for DvRd(Ni) using the MST parameters obtained using the DvRd(Ni) NMR structure is shown in Fig. 4a.

### Estimation of contact shifts in DvRd(Ni)

To estimate the contact shift contributions to the observed chemical shifts, the diamagnetic and PCS contributions must be factored out ($\delta_{fc} = \delta_{exp} - \delta_{psc} - \delta_{dia}$). Using the calculated MSTs from the NMR data from DvRd(Ni) and the coordinates from the DvRd(Ni) NMR structure and the

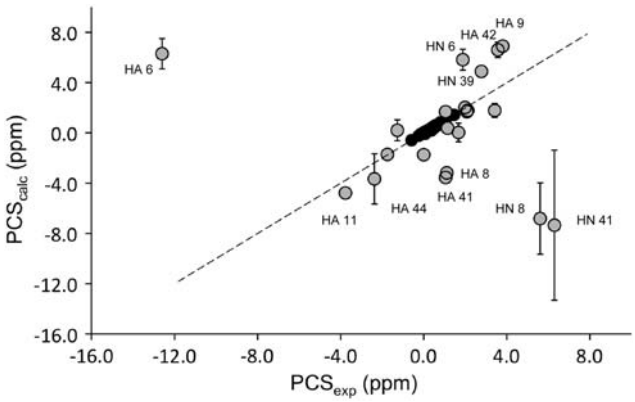


**Fig. 3** The calculated versus experimental pseudocontact shifts for DvRd(Ni). The data were obtained using the magnetic susceptibility anisotropy tensor calculated from the mean solution structure and backbone chemical shifts excluding those from any nucleus within eight covalent bonds of the metal centre (*black circles*). Also shown are the experimental and average calculated pseudocontact shifts [using the DvRd(Fe), the Ni(II) form of *Clostridium pasteurianum* rubredoxin (CpRd) and mean NMR structures] from backbone nuclei within eight covalent bonds (*grey circles*). The *error bars* are the standard deviations for the results from the three structures. The equation of the line is $y = 0.984x - 0.005$, with $R^2$ of 0.98. *PCS* pseudocontact shift

DvRd(Fe) and CpRd(Ni) X-ray structures, we calculated the PCS contribution to the chemical shift of nuclei close to the metal centre. These PCSs (see the electronic supplementary material) and the chemical shifts from the diamagnetic zinc form of DvRd were subtracted from the observed chemical shifts to estimate the contact shift contribution in DvRd(Ni).

Table 3 shows the average (from the three structures) estimated contact shifts (and the standard deviation) for the $^1$H nuclei within seven bonds (covalent and/or hydrogen bond) of the Ni(II) atom. The nuclei included in the table and the numbers in parentheses, which indicate the number of bonds removed from the metal centre, assume that the hydrogen-bonding pattern at the metal centre (Fig. 5) is of the standard rubredoxin type [16].

## Discussion

### The solution structures of DvRd(Zn) and DvRd(Ni)

The backbone conformation of the Zn form of DvRd is very similar to the backbone fold of the X-ray structure of DvRd(Fe), as expected. In fact, the global fold of rubredoxins is conserved in almost all organisms: the maximum RMSD for the backbone alignment of the high-resolution (0.5–1.5-Å) X-ray structures for *P. furiosus*, *C. pasteurianum*, *D. gigas*, *D. vulgaris*, *P. abyssi* and *D. desulfuricans* is 1.5 Å$^2$.

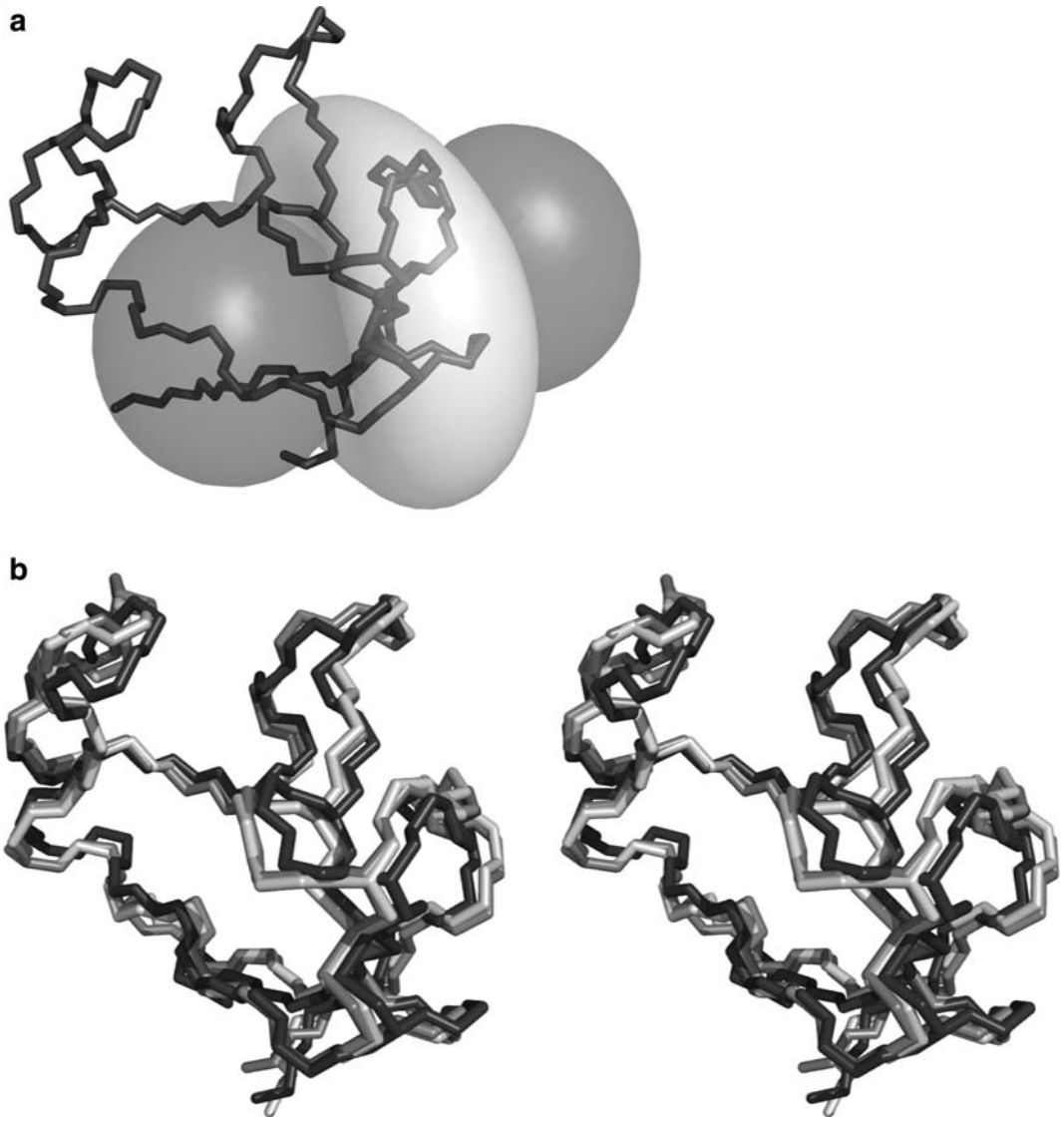


**Fig. 4** **a** A pseudocontact chemical shift isosurface at −1 ppm (*dark grey*) and +1 ppm (*light grey*) using the magnetic susceptibility anisotropy tensor parameters obtained from the DvRd(Ni) NMR structure. **b** A stereo overlay plot of the backbone and metal centre for the X-ray structures of DvRd(Fe) (*dark grey*) and CpRd(Ni) (*light grey*) and the mean NMR structure for DvRd(Ni) (*black*)

The solution structure of the Ni(II) form has a relatively good global backbone RMSD, with poorer definition near the paramagnetic Ni(II) centre, especially the C6–C9 region, owing to a lack of experimental NOE constraints. The backbone RMSD, excluding the N-terminus, from the X-ray structure of the Fe form is 1.09 $Å^2$. The backbone RMSD of the solution structures of the Zn(II) and Ni(II) forms is 1.6 $Å^2$. A comparison with the published X-ray structure of CpRd(Ni) indicates that the backbone conformation is very similar (backbone RMSD, residues 1–52, 1.1 $Å^2$, Fig. 4b). The RMSD per residue for these comparisons is shown in the electronic supplementary material. Comparison of the geometry at the metal centre is more problematic owing to the poorer definition in the NMR structure; however, as the sequences of CpRd and DvRd differ only slightly near the binding cysteines (DvRd –CTVC–//–CPVCGA– and CpRd –CTVC–//–CPLCGV–), the backbone geometries would be expected to be similar.

The hydrogen-bonding network at the metal centre in rubredoxins is well known and includes a number of NH–S$\gamma$ hydrogen bonds (Fig. 5). To probe the hydrogen bonding in DvRd(Ni), NH–S$\gamma$ distances in the family of solution structures were measured. It was found that two of the six NH–S$\gamma$ hydrogen bonds present in most rubredoxins, Y11-C9 and V41-C39, had longer distances than normally found: 4.50(0.54) and 3.01(0.29) Å. To confirm the

**Table 3** The estimated contact shifts for all $^{1}$H nuclei within seven bonds (covalent and/or hydrogen bonds and assuming a standard rubredoxin hydrogen-bonding pattern at the metal centre [16]) of the Ni(II) atom

| Covalent | NH–O | NH–S | $\delta_{con}$ | SD | Covalent | NH–O | NH–S | $\delta_{con}$ | SD |
|---|---|---|---|---|---|---|---|---|---|
| V5 | | | | | V38 | | | | |
| Hα (7) | | | −0.03 | 0.1 | Hα (7) | | | 0.39 | 0.1 |
| C6 | | | | | C39 | | | | |
| HN (5) | | | −3.94 | 1.2 | HN (5) | | HN (7)[a] | −2.11 | 0.3 |
| Hα (4) | | | −18.89 | 1.2 | Hα (4) | | | ND | |
| Hβ (3) | | | 168.5 | 5.7 | Hβ (3) | | | 164.0 | 4.9 |
| | | | 124.0 | 6.3 | | | | 139.09 | 4.3 |
| T7 | | | | | P40 | | | | |
| HN (6) | | HN (7) | −1.48 | 0.8 | Hα (7) | | Hα (6) | 1.65 | 0.7 |
| Hα (7) | | Hα (6) | 0.78 | 0.2 | | | | | |
| V8 | | | | | V41 | | | | |
| | | HN (2 + 7) | 12.43 | 2.8 | | | HN (2 + 7) | 13.64 | 5.7 |
| Hα (7) | | Hα (5 + 6) | 4.61 | 0.3 | Hα (7) | | Hα (5 + 6) | 4.29 | 0.3 |
| C9 | | | | | C42 | | | | |
| HN (5) | | HN (2 + 7) | ND | | HN (5) | | HN (2 + 7) | ND | |
| Hα (4) | | Hα (5) | −3.10 | 0.3 | Hα (4) | | Hα (5) | −3.03 | 0.6 |
| Hβ (3) | | Hβ (6) | 325.8 | 4.8 | Hβ (3) | | Hβ (6) | 326.1 | 4.5 |
| | | | 264.5 | 1.4 | | | | 257.4 | 1.2 |
| G10 | | | | | G43 | | | | |
| HN (6) | HN (6) | HN (7 + 7) | ND | | HN (6) | HN (6) | HN (7 + 7) | ND | |
| Hα (7) | | Hα (6) | ND | | Hα (7) | | Hα (6) | 1.64 | 0.6 |
| | | | | | | | | 0.34 | 0.4 |
| Y11 | | | | | A44 | | | | |
| | | HN (2) | ND | | | | | | |
| | | Hα (5) | 1.01 | 0.2 | | | Hα (5) | 1.28 | 2.0 |
| E12 | | | | | E50 | | | | |
| | | HN (7) | −0.03 | 0.2 | | HN (7) | | 0.39 | 0.1 |

The number of bonds that separate each nucleus from the Ni(II) atom is presented in *parentheses*. The contact shifts presented (with standard deviations) are average values calculated using the mean NMR solution structure and the X-ray structure from CpRd(Ni) and DvRd(Fe)

*SD* standard deviation, *ND* not detected

[a] Via NH(39)–O(44)

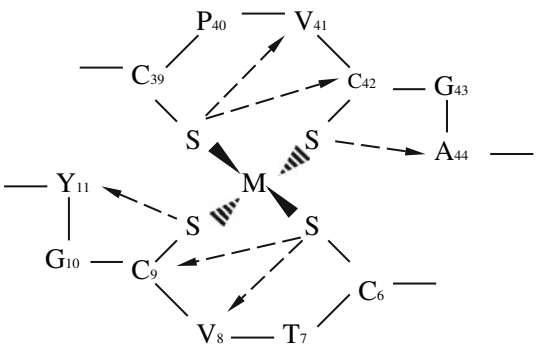


**Fig. 5** Representation of the NH–Sγ hydrogen-bonding network found at the metal centre in rubredoxins. *Arrows* indicate the Sγ to NH direction. The amino acid numbering is for DvRd. (Adapted from [19])

presence of these hydrogen bonds, an analysis of the contact shift contribution to the observed chemical shifts in DvRd(Ni) was carried out.

## Contact shifts in DvRd(Ni)

The estimation of contact shifts requires that the PCS and diamagnetic contributions be known. As Ni(II) has no accessible diamagnetic oxidation state, another diamagnetic metal must be used. Zn(II) is a good candidate as it adopts a tetrahedral coordination and Zn–S bond lengths are comparable to Ni–S bond lengths. Figure 3 shows how the calculated PCSs for a number of backbone chemical shifts deviate from their experimental values. The error

bars shown in Fig. 3 are the standard deviations for the calculated PCSs using the solution structure and the two X-ray structures for DvRd(Fe) and CpRd(Ni). The largest standard deviations are seen for HA from residue 44 and HN for residues 8 and 41. The variations for HN 8 and HN 41 result from structural differences between the solution and X-ray structures. This is most probably due to the poor definition, due to the lack of experimental constraints, in the solution structure for the backbone near the Ni(II) centre. In fact the standard deviation for calculated PCSs between the DvRd(Fe) and CpRd(Ni) X-ray structures for these atoms is 0.24 and 0.29, respectively, compared with 2.8 and 6.0 for all three structures (Table 3). For HA 44 the standard deviation does not change significantly when considering the X-ray structures alone (2.0 compared with 1.7). However, even assuming that the solution structure may not be well defined near the Ni(II) centre, structural differences alone do not explain the deviations of the calculated PCSs from their experimental values. Contact shift contributions to the observed chemical shifts, however, can be used to explain these deviations.

A number of studies, both experimental and theoretical, have shown the importance of hydrogen bonds (NH–O and NH–S) in rubredoxin and changes in hydrogen-bond strength have been found to modulate the redox potential of the active site [16]. The presence of these hydrogen bonds, especially NH–S, at the metal centre can be confirmed for DvRd(Ni) in solution by considering the pattern of contact shifts shown in Table 3. Contact shifts result from the presence of unpaired electron spin density at a nucleus and it is assumed that the larger the contact shift the more unpaired electron spin density resides at a nucleus. This proportionality is valid for a single electron in an orbital which is well separated from any other excited level. This spin density can arrive via covalent bonds or via hydrogen bonds. For DvRd(Ni), most of the larger contact shifts (more than 2 ppm) in Table 3 can be explained by invoking a hydrogen-bonding network near the Ni(II) centre that facilitates unpaired electron spin delocalization. Appreciable contact contributions to observed chemical shifts are seen here for protons up to five covalent bonds removed from the Ni(II) atom and importantly for atoms further than five covalent bonds from Ni(II). For instance, the $^{1}$H NH resonances for V8 and V41 are both eight covalent bonds removed from the Ni(II) atom but have contact shifts of 12.43 and 13.64 ppm, respectively. These large contact shifts can be explained by the fact that they are also involved in NH–S hydrogen bonds to Ni-ligating S$\gamma$ atoms. Also, for the NH protons of C9 and C42 the unpaired electron spin density from the Ni(II) atom arrives via five covalent bonds and via two bonds involving an NH–S hydrogen bond (Table 3), resulting in these resonances being undetectable under our experimental conditions. Conversely, the NHs of C6 and C39 are not involved in NH–S hydrogen bonds and only receive unpaired electron spin density via five covalent bonds and are therefore detectable.

These contact shift results confirm the V8-C6, C9-C6, C42-C39 and A44-C42 NH–S hydrogen bonds seen in the DvRd(Ni) solution structure. They also confirm that the V41-C39 NH–S hydrogen bond is present as well, something that could not be confirmed using the solution structure alone. The final Y11-C9 NH–S hydrogen bond was not detected in the solution structures, and the Y11 $^{1}$H NH resonance could not be detected under our experimental conditions. However, this fact in combination with the results of Wilkens et al. [19], where density functuonal theory calculations indicated the nitrogen of Tyr11 as having the largest calculated contact electron density and the shortest NH–S hydrogen bond in a CpRd(Fe) structure, and of Lin et al. [23], where the $^{15}$N resonance of Y11 in oxidized CpRd(Fe) was the most low field shifted of all the $^{15}$N hyperfine signals, suggests that the absence of this NH resonance may be due to relaxation broadening or a large hyperfine shift due to unpaired electron spin density arriving via an NH–SH bond.

The use of NMR, more specifically a combination of experimental chemical shifts from paramagnetic and diamagnetic forms of DvRd in combination with available structures, allows the distribution of unpaired electron spin density to be determined from contact shifts and hydrogen-bonding networks to be inferred even in regions close to the metal where there is a lack of experimental constraints.

## Analysis of the H$\beta$ shifts from the binding cysteines in DvRd(Ni)

To determine the amount of electron spin density present at the H$\beta$ nuclei, the average chemical shift of an H$\beta$ proton pair ($\delta_{1/2}$) is often used [55] as is it less sensitive to conformational changes in the H$\beta$–C$\beta$–S$\gamma$–M dihedral angle [56]. The $\delta_{1/2}$ values for the H$\beta$ proton pairs in DvRd(Ni) and CpRd(Fe) show (Table 1) that C9 (321/320 ppm) and C42 (320/321 ppm) have much higher electron spin density present at the nucleus than C6 (183 ppm) and C39 (178 ppm). A comparison of experimental NMR data with density functional calculations for the hyperfine shifts in oxidized and reduced CpRd(Fe) showed that NH–S hydrogen bonds are very effective in transferring electron spin density from the metal to other nuclei and that small changes in NH–S hydrogen-bond distances create large changes in spin density at the resonating nuclei [18]. Intuitively, as the S$\gamma$ atoms for C6 and C39 have two NH atoms hydrogen-bonded, they may be expected to have less electron spin density owing to these "extra" outlets for spin delocalization when compared with the S$\gamma$ atoms (and attached nuclei) for C9 and C42, which only have one NH–S hydrogen bond each. The experimental $\delta_{1/2}$ values for

DvRd(Ni) confirm that the H$\beta$ protons of C9 and C42 have higher unpaired electron spin density compared with C6 and C39 and that the same electron spin delocalization (hydrogen-bond) pathway may be active here. This type of pattern is also seen for oxidized and reduced CpRd(Fe), where the $^{2}$H hyperfine shifts for C9 and C42 were seen further downfield (Table 1) than those for C6 and C39 [19].

In general, it appears that for a paramagnetic metal bound to cysteine in rubredoxin, the spin density on the cysteine H$\beta$ nuclei depends not only on the H$\beta$–C$\beta$–S$\gamma$–M dihedral angle, but also on the number of NH–S hydrogen bonds to the S$\gamma$ atom: two NH–S hydrogen bonds compared with one allow more electron spin density to be siphoned off, resulting in lower $\delta_{1/2}$ values for the corresponding H$\beta$ protons. NH–S hydrogen bonds are also present in blue Cu proteins and their derivatives where one ligating cysteine is present with approximately the same dihedral angle. NMR chemical shift data is available for a number of Ni(II) derivatives along with structural data from the native Cu forms. Table 1 presents the $\delta_{1/2}$ values for the cysteine H$\beta$ protons for Ni(II) forms of azurin [33, 34], pseudoazurin [35], stellacyanin [36], umecyanin [37] and amicyanin [34], and it can be seen that the presence of NH–S hydrogen bonds may be correlated to a decrease in $\delta_{1/2}$ values. Those cysteine H$\beta$ protons whose S$\gamma$ atom has two hydrogen bonds appear at higher field. It must be remembered, however, that other factors such as differences in M–S bond strength/length and the presence of axial ligands will also affect chemical shifts and may also play a role in these cases [34, 37].

## Conclusions

The large number of NMR studies using diamagnetic and paramagnetic forms of the small Fe–S protein rubredoxin to validate theoretical calculations, test new pulse sequences and probe unfolding pathways confirm rubredoxin as an important metalloprotein model system. In this work the Ni(II) form of this protein was studied not only because it acts as a model for Ni(II)-containing enzymes, but also because Ni(II), owing to its relaxation properties, allows more of the protein to be seen by NMR compared with the native Fe form. Initially, solution structures of the Zn(II) and Ni(II) forms of DvRd were determined by NMR. The assignment of the spectra of the paramagnetic Ni(II) form required the use of tailored NMR experiments in conjunction with the MST obtained via PCSs. The structure of the Ni(II) form was subsequently determined using constraints from standard 2D/3D spectra, 1D NOE difference spectra and PCS data. The structures were found to be very similar to the numerous published rubredoxin structures obtained using NMR and X-rays.

To probe the geometry and hydrogen-bonding network at the metal centre, the contact shifts for the observable resonances near the Ni(II) centre were determined by subtracting the experimental diamagnetic and calculated dipolar (PCS) shifts from the observed chemical shifts. The subsequent pattern of contact shifts for DvRd(Ni) observed in solution can be explained by invoking a hydrogen-bond network similar to that seen in a published low-resolution X-ray structure from CpRd(Ni). The results also confirm the importance of the NH–S hydrogen bonds in the distribution of electron spin density in rubredoxin and show how structural information can be obtained from the distribution of contact shifts even when there is a lack of experimental NOE constraints.

Analysis of the contact-shift-dominated $\delta_{1/2}$ values from the cysteine H$\beta$ protons shows how NH–S hydrogen bonds as well as H$\beta$–C$\beta$–S$\gamma$–M dihedral angles are important in unpaired electron spin density delocalization on these atoms. A S$\gamma$ atom involved in two NH–S hydrogen bonds results in electron spin density being siphoned off and an observed shift for the H$\beta$ protons of C6 and C39 of approximately 150–200 ppm. The presence of one NH–S hydrogen bond to a S$\gamma$ atom results in more electron spin density at the H$\beta$ protons as is the case for C9 and C42 (shifts of approximately 300–250 ppm). This type of analysis can also be applied to the H$\beta$ protons from the single ligating cysteine ligand found in the Ni(II) forms of azurin and azurin-type Cu proteins. Here a similar correlation between the $\delta_{1/2}$ values of the H$\beta$ protons and the number of NH–S hydrogen bonds (for the same H$\beta$–C$\beta$–S$\gamma$–M dihedral angles) was found, suggesting that hydrogen bonds of this type may also play a role in the distribution/delocalization of electron spin density in these native Cu proteins as well.

**Acknowledgments** This work was supported by the Fundação para a Ciência e Tecnologia POCI/QUI/57741/2004 (J.J.G.M.) and FEDER in Portugal (BD/13879/97, S.G.N.). I.D. thanks CICECO for a young researcher grant. Work in Madison was supported by NIH grants R01 GM 58667 (J.L.M.) and P41 RR02301 (J.L.M.), which supports the National Magnetic Resonance Facility at Madison.

## References

1. Bonisch H, Schmidt C, Bianco P, Ladenstein R (2005) Acta Crystallogr Sect D Biol Crystallogr 61:990–1004
2. Chen C, Lin Y, Huang Y, Liu M (2006) Biochem Biophys Res Commun 349:79–90
3. Bertini I, Kurtz D, Eidsness M, Liu G, Luchinat C, Rosato A, Scott R (1998) J Biol Inorg Chem 3:401–410
4. Moura I, Teixeira M, Legall J, Moura J (1991) J Inorg Biochem 44:127–139
5. Bertini I, Luchinat C, Parigi G, Pierattelli R (2005) Chembiochem 6:1536–1549

6. Otting G (2008) J Biomol NMR 42:1–9. doi:10.1007/s10858-008-9256-0
7. Gaponenko V, Sarma SP, Altieri AS, Horita DA, Li J, Byrd RA (2004) J Biomol NMR 28:205–212
8. Gaponenko V, Altieri AS, Li J, Byrd RA (2002) J Biomol NMR 24:143–148
9. Wang J, Valafar H, Prestegard J (2005) J Magn Reson 172:85–90
10. Prestegard JH, Bougault CM, Kishore AI (2004) Chem Rev 104:3519–3540
11. Bougault C, Eidsness M, Prestegard J (2003) Biochemistry 42:4357–4372
12. Zartler E, Jenney F, Terrell M, Eidsness M, Adams M, Prestegard J (2001) Biochemistry 40:7279–7290
13. Tian F, Valafar H, Prestegard J (2001) J Am Chem Soc 123:11791–11796
14. Tian F, Fowler CA, Zartler ER, Jenney FA, Adams MW, Prestegard JH (2000) J Biomol NMR 18:23–31
15. Al-Hashimi H, Valafar H, Terrell M, Zartler E, Eidsness M, Prestegard J (2000) J Magn Reson 143:402–406
16. Lin IJ, Gebel EB, Machonkin TE, Westler WM, Markley JL (2005) Proc Natl Acad Sci USA 102:14581–14586
17. Lin IJ, Gebel EB, Machonkin TE, Westler WM, Markley JL (2003) J Am Chem Soc 125:1464–1465
18. Wilkens SJ, Xia B, Volkman BF, Weinhold F, Markley JL, Westler WM (1998) J Phys Chem B 102:8300–8305
19. Wilkens SJ, Xia B, Weinhold F, Markley JL, Westler WM (1998) J Am Chem Soc 120:4806–4814
20. Xia B, Wilkens SJ, Westler WM, Markley JL (1998) J Am Chem Soc 120:4893–4894
21. Xia B, Westler WM, Cheng H, Meyer J, Moulis J, Markley JL (1995) J Am Chem Soc 117:5347–5350
22. Volkman BF, Wilkens SJ, Lee AL, Xia B, Westler WM, Beger R, Markley JL (1999) J Am Chem Soc 121:4677–4683
23. Lin IJ, Xia B, King DS, Machonkin TE, Westler WM, Markley JL (2009) J Am Chem Soc 131:15555–15563
24. LeMaster D, Minnich M, Parsons P, Anderson J, Hernandez G (2006) J Inorg Biochem 100:1410–1412
25. Harrop T, Mascharak P (2006) Model complexes of Ni-containing enzymes. Wiley, Weinheim
26. Pochapsky T, Pochapsky S, Ju T, Mo H, Al-Mjeni F, Maroney M (2002) Nat Struct Biol 9:966–972
27. Dardel F, Ragusa S, Lazennec C, Blanquet S, Meinnel T (1998) J Mol Biol 280:501–513
28. Banci L, Bertini I, Calderone V, Ciofi-Baffoni S, Mangani S, Martinelli M, Palumaa P, Wang S (2006) Proc Natl Acad Sci USA 103:8595–8600
29. Maher M, Cross M, Wilce M, Guss J, Wedd A (2004) Acta Crystallogr Sect D Biol Crystallogr 60:298–303
30. Moratal J, Salgado J, Donaire A, Jimenez H, Castells J, Martinezferrer M (1993) Magn Reson Chem 31:S41–S46
31. Salgado J, Jimenez H, Moratal J, Kroes S, Warmerdam G, Canters G (1996) Biochemistry 35:1810–1819
32. Hannan J, Davy S, Moore G, Eady R, Andrew C (1998) J Biol Inorg Chem 3:282–291
33. Donaire A, Salgado J, Moratal J (1998) Biochemistry 37:8659–8673
34. Salgado J, Kalverda A, Diederix R, Canters G, Moratal J, Lawler A, Dennison C (1999) J Biol Inorg Chem 4:457–467
35. Dennison C, Sato K (2002) Inorg Chem 41:6662–6672
36. Fernandez C, Sannazzaro A, Diaz L, Vila A (1998) Inorg Chim Acta 273:367–371
37. Dennison C, Harrison M (2004) J Am Chem Soc 126:2481–2489
38. Bruschi M, Hatchikian EC, Legall J, Moura JJG, Xavier AV (1976) Biochim Biophys Acta 449:275–284
39. Goodfellow BJ, Nunes SG, Rusnak F, Moura I, Ascenso C, Moura JJG, Volkman BF, Markley JL (2002) Protein Sci 11:2464–2470
40. Delaglio F, Grzesiek S, Vuister GW, Zhu G, Pfeifer J, Bax A (1995) J Biomol NMR 6:277–293
41. Goddard T, Kneller D
42. Bartels C, Xia T-H, Billeter M, Güntert P, Wüthrich K (1995) J. Biomol NMR 5:1–10
43. Wishart DS, Bigam CG, Yao J, Abildgaard F, Dyson HJ, Oldfield E, Markley JL, Sykes BD (1995) J Biomol NMR 6:135–140
44. Inubushi T, Becker ED (1983) J Magn Reson 51:128–133
45. Macedo AL, Palma PN, Moura I, Legall J, Wray V, Moura JJG (1993) Magn Reson Chem 31:S59–S67
46. Bertini I, Briganti F, Luchinat C, Messori L, Monnanni R, Scozzafava A, Vallini G (1991) FEBS Lett 289:253–256
47. Herrmann T, Güntert P, Wüthrich K (2002) J Mol Biol 319:209–227
48. Banci L, Bertini I, Cremonini MA, Gori-Savellini G, Luchinat C, Wüthrich K, Güntert P (1998) J Biomol NMR 12:553–557
49. Güntert P, Mumenthaler C, Wüthrich K (1997) J Mol Biol 273:283–298
50. Banci L, Bertini I, Bren KL, Cremonini MA, Gray HB, Luchinat C, Turano P (1996) J Biol Inorg Chem 1:117–126
51. Schmitz C, Stanton-Cook MJ, Su XC, Otting G, Huber T (2008) J Biomol NMR 41:179–189. doi:10.1007/s10858-008-9249-z
52. DeLano W (2002)
53. Pintacuda G, Keniry MA, Huber T, Park AY, Dixon NE, Otting G (2004) J Am Chem Soc 126:2963–2970
54. Bertini I, Luchinat C, Parigi G, Pierattelli R (2008) Dalton Trans 3782–3790
55. Fernandez CO, Niizeki T, Kohzuma T, Vila AJ (2003) J Biol Inorg Chem 8:75–82
56. Fernandez CO, Sannazzaro AI, Vila AJ (1997) Biochemistry 36:10566–10570